Supporting Information

Cation-Deficient Spinel $ZnMn_2O_4$ Cathode in $Zn(CF_3SO_3)_2$ Electrolyte for Rechargeable Aqueous Zn-Ion Battery

Ning Zhang,[†] Fangyi Cheng,[,†,‡] Yongchang Liu,[†] Qing Zhao,[†] Kaixiang Lei,[†] Chengcheng Chen,[†] Xiaosong Liu,[∥] and Jun Chen[†,‡]*

[†]Key Laboratory of Advanced Energy Materials Chemistry (Ministry of Education) and State Key Laboratory of Elemento-Organic Chemistry, College of Chemistry, Nankai University, Tianjin 300071, China

[‡]Collaborative Innovation Center of Chemical Science and Engineering, Nankai University, Tianjin 300071, China

[∥]State Key Laboratory of Functional Materials for Informatics, Shanghai Institute of Microsystem and Information Technology, Chinese Academy of Sciences, Shanghai 200050, China

Synthesis of neat $ZnMn_2O_4$ via conventional ceramic method:

In a typical synthesis, 5 mL 0.2 M $Zn(NO_3)_2$ and 10 mL 0.2 M $Mn(NO_3)_2$ were dissolved in 10 mL deionized water. After adding 6.4 mmol citric acid, the solution was neutralized by 1.2 mL 25 wt.% aqueous ammonia solution. Under magnetic stirring, 50 mL absolute ethanol was poured into the mixed solution. The water and ethanol liquid were evaporated in an airing oven at 100 ^oC to get the gel-like precursor. The final spinel product was obtained by heating the precursors at 600 ^oC for 10 h in air atmosphere. The as-prepared $ZnMn_2O_4$ shows a nanoparticulate morphology with average particle size of ~50 nm. For comparison, neat ZMO with smaller particle size of ~23 nm was prepared by adopting similar procedures except diluting the precursor solution from 0.2 M to 0.05 M.

Chemical titration

The cation vacancies and the oxidation state of Mn were determined by chemical titration.[1-4] Typically, the as-prepared samples (10 mg) were dissolved in 15 mL 0.5 M H_2SO_4 and 10 mL 83 wt% H_3PO_4 with an excess of 0.0765 M $Fe(NH_4)_2(SO_4)_2$ solution. The mixed solution was titrated with calibrated 0.00947 M $KMnO_4$ solution. The corresponding reactions of chemical titration include:

$$ZnMn_{2-x}O_4 + (2+2x)\,Fe^{2+} + 8H^+ = Zn^{2+} + (2-x)\,Mn^{2+} + (2+2x)\,Fe^{3+} + 4H_2O \quad \text{(S1)}$$

$$MnO_4^- + 5Fe^{2+} + 8H^+ = Mn^{2+} + 5Fe^{3+} + 4H_2O \quad \text{(S2)}$$

The x value of $ZnMn_{2-x}O_4$ was calculated according to eqations S3-S5:

$$x = \frac{50 \times M \times (0.0765V_1 - 0.04735V_2)}{W_t} - 1 \quad \text{(S3)}$$

$$M = 129.38+(2-x)\times 54.93 \quad \text{(S4)}$$

$$x = \frac{11962 \times (0.0765V_1 - 0.04735V_2) - W_t}{2746.5 \times (0.0765V_1 - 0.04735V_2) + W_t} \quad \text{(S5)}$$

where M is the molar mass of $ZnMn_{2-x}O_4$, V_1 is the consumption volume of $Fe(NH_4)_2(SO_4)_2$ solution and V_2 is the consumption volume of the $KMnO_4$ solution. W_t is the the weight percentage of

$ZnMn_{2-x}O_4$ in as-prepared samples.

GITT measurements and the calculation of the diffusion coefficient

Before the GITT measurement, the assembled cells were first charged/discharged at 20 mA g^{-1} for one cycle to stablize the cells. The current pulse lasted for 30 min at 50 mA g^{-1} and then the cell was relaxed for 60 min to make the volatge reach the equilibrium. These procedures were repeatedly applied to the cell during the entire charge/discharge process. The chemical diffusion coefficient of Zn^{2+} can be calculated based on the following equation:[5,6]

$$D_{GITT} = \frac{4}{\pi}\left(\frac{m_B V_m}{M_B S}\right)^2\left(\frac{\Delta E_S}{\tau(dE_\tau/d\sqrt{\tau})}\right)^2 \approx \frac{4}{\pi\tau}\left(\frac{m_B V_m}{M_B S}\right)^2\left(\frac{\Delta E_S}{\Delta E_\tau}\right)^2 \quad \left(\tau \ll \frac{L^2}{D_{GITT}}\right) \tag{S6}$$

where τ is the duration time of the current pulse, m_B is the mass of the active material, M_B is the molecular weight (g/mol) and V_m is its molar volume (cm^3/mol), S is the total contacting area of electrode with electrolyte, $dE_\tau/d\sqrt{\tau}$ is the slope of the linearized region of the potential E_τ during the current pulse of duration time τ, ΔE_s is the difference in the open circuit voltage measured at the end of the relaxation period for two successive steps, and L is the thickness of electrode. The equation can be simplified as the right hand of the equation if $\Delta E_\tau/\tau^{1/2}$ shows a linear relationship.

Electrical conductivity measurements

Around 150 mg sample powders were pressed at 20 MPa into a chip with diameter of 1.0 cm and thickness of 0.05 cm. Two stainless steel electrodes (1.6 cm in diameter, 0.2 cm in thickness) were placed onto the two faces of the as-prepared chip, which were held by a clip. For comparison, the $ZnMn_2O_4$+C sample was prepared by mixing 90 mg $ZnMn_2O_4$ and 60 mg Vulcan XC-72 carbon. The resistivity test was performed using Ametek Parstat 4000 and resistance values (R) were determined by voltmeter-ammeter method. A stainless steel chip (1.6 cm in diameter, 0.2 cm in thickness, resistivity of 6.9×10^{-7} Ω•m) was used as the reference. The conductivity κ was deduced using relation: $\kappa = 1/\rho = d/(R\times S)$, where ρ, d and S represent the resistivity, surface area and thickness of the chip.

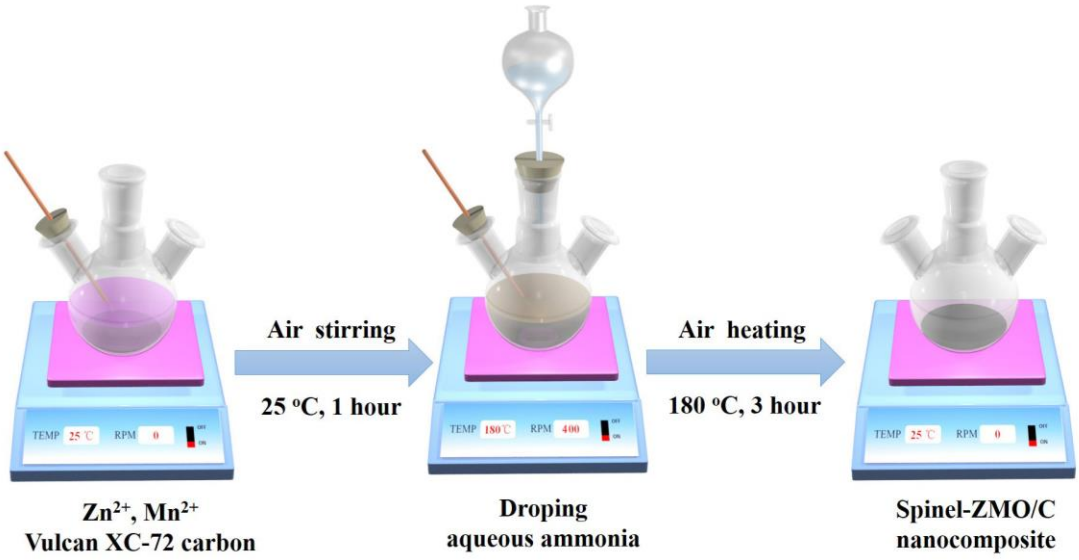

Figure S1. Schematic illustration of the synthesis of ZMO/C nanocomposite. The synthesis involves two steps of oxidation precipitation and spinel crystallization under mild condition.

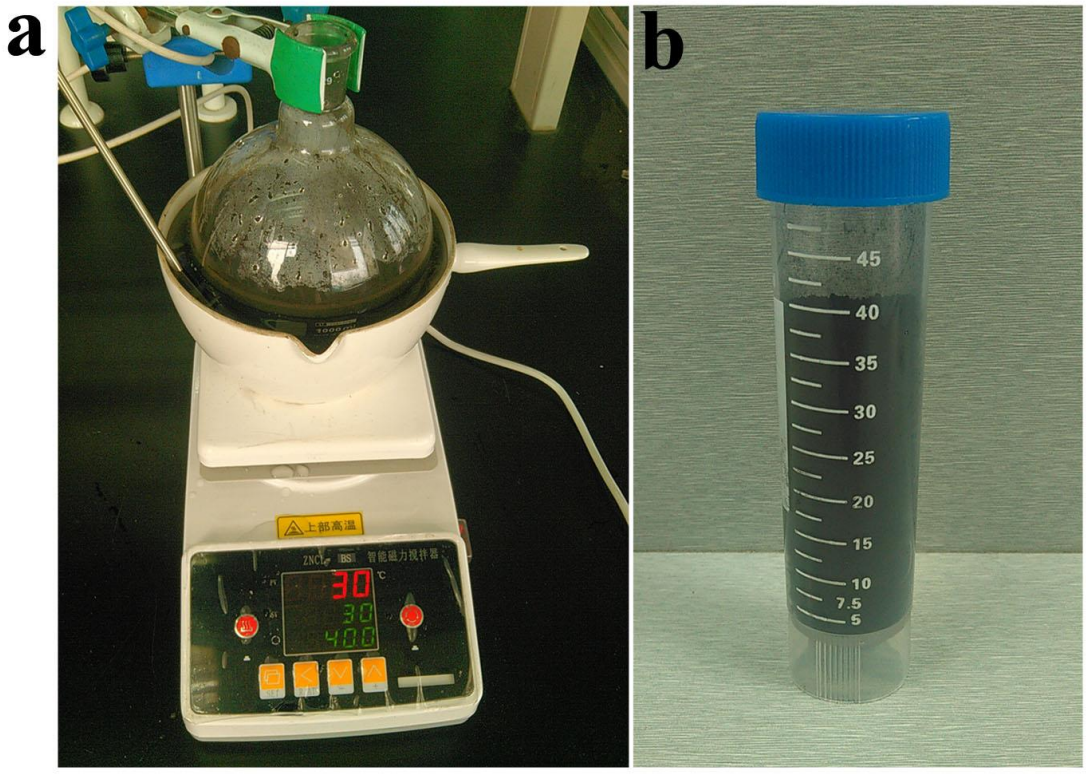

Figure S2. Digital photographs of (a) synthesis equipment and (b) as-prepared sample in ~100 g scale.

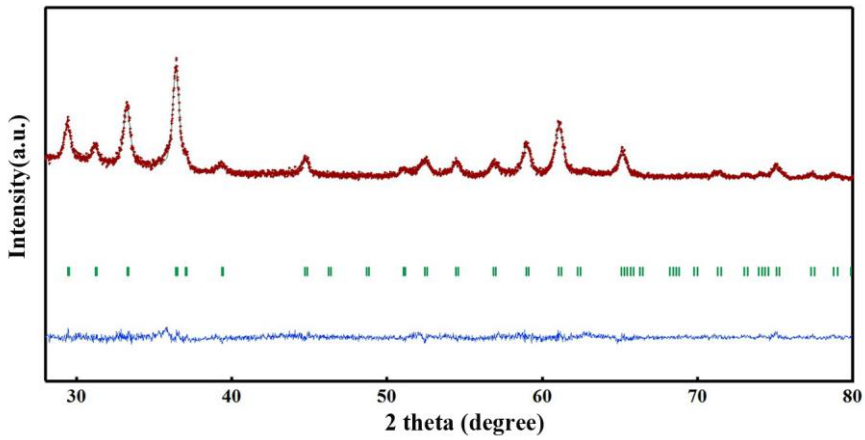

Figure S3. Rietveld refined XRD data of neat spinel $ZnMn_2O_4$ synthesized at 600 ^oC. Experimental data, calculated profiles, allowed Bragg diffraction positions and difference curve are marked with red dots, cyan line, vertical bars and blue line, respectively. Refined results of Figure 1a and Figure S3 are summarized in Table S1 and S2, respectively.

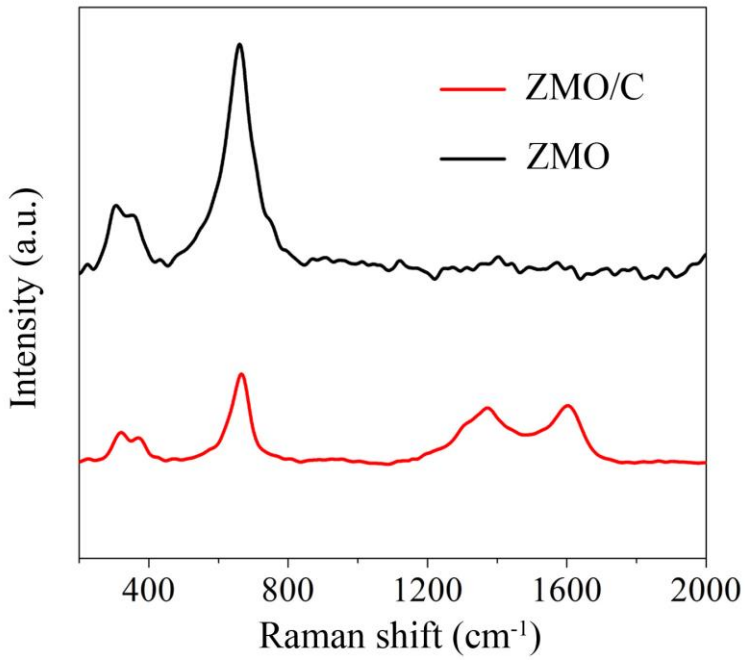

Figure S4. Raman spectra of ZMO/C and neat ZMO.

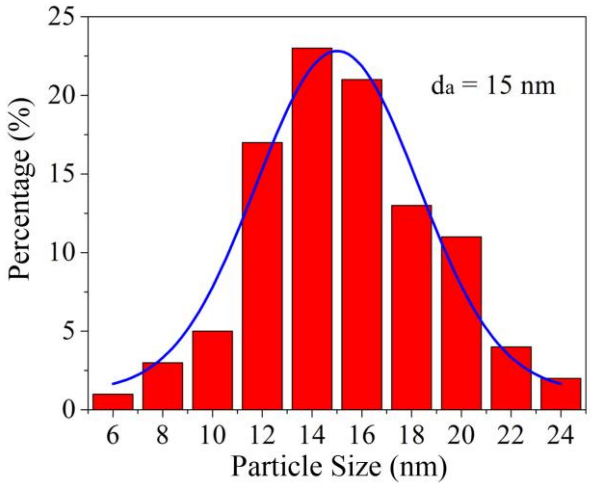

Figure S5. Particle size distribution of ZMO/C.

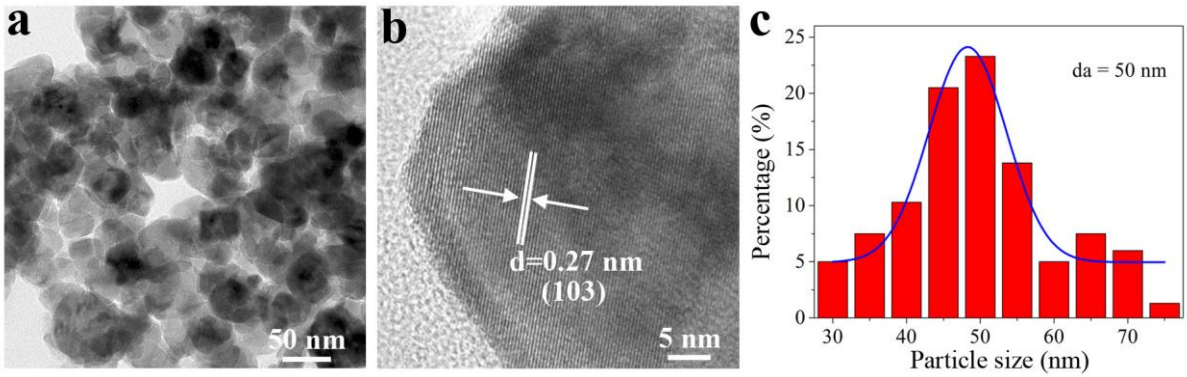

Figure S6. (a) TEM image, (b) HRTEM image and (c) Particle size distribution of neat ZMO prepared at 600 ^{o}C.

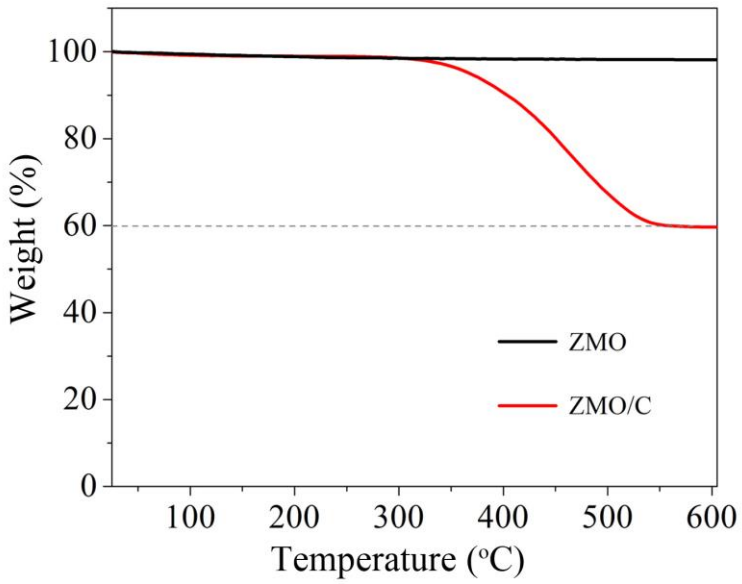

Figure S7. TG analysis of as-prepared ZMO/C and neat ZMO. TG analysis was tested in air from room temperature to 600 °C at 5 °C min^{-1}. The carbon content of as-prepared ZMO/C is 40 wt%. As expected, negligible mass loss was observed up to 600 °C for neat ZMO.

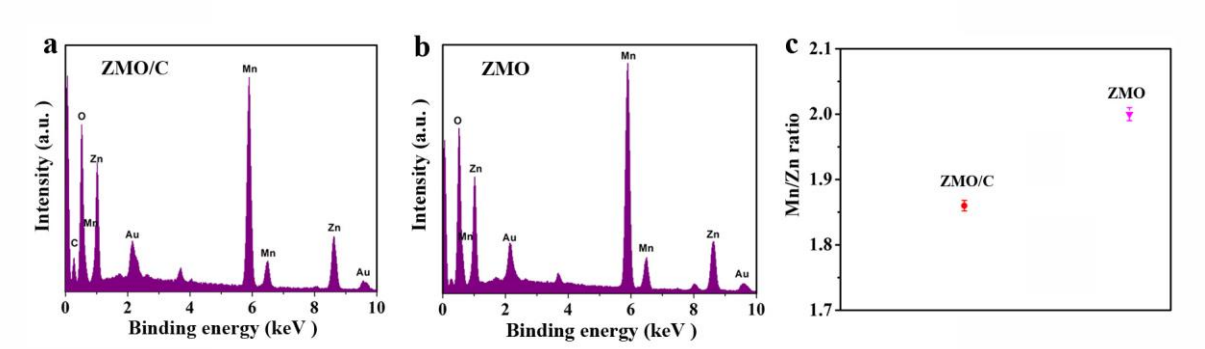

Figure S8. EDS of as-prepared (a) ZMO/C and (b) neat ZMO. (c) Determined Mn/Zn ratio of the samples. Error bar represents deviation of at least three measurements.

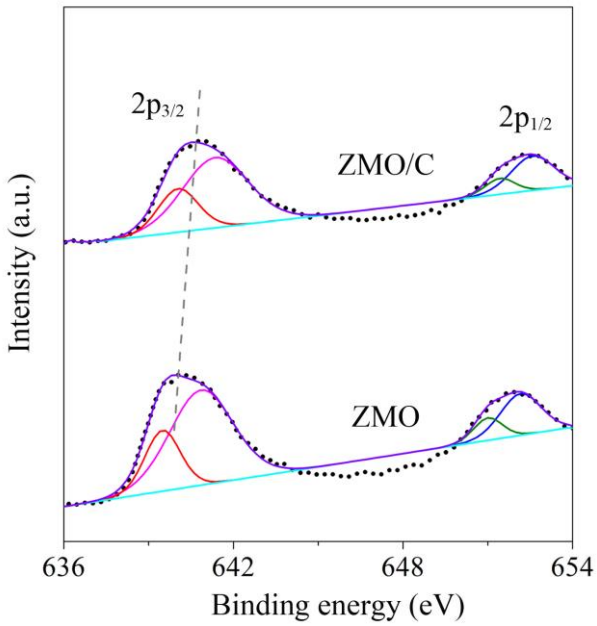

Figure S9. Mn 2p XPS spectra of the synthesized samples. The dot lines are the experimental data. The fitting of two deconvoluted peaks in Mn 2p spectra suggests the presence of multiple Mn valence.

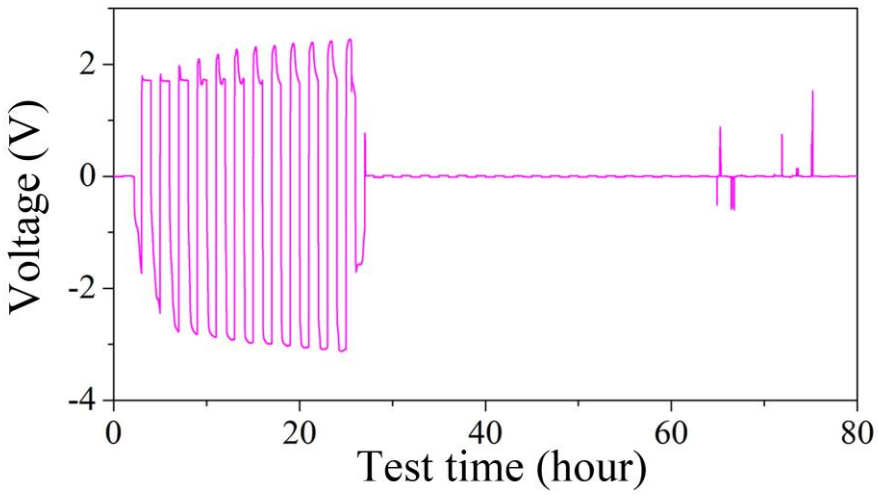

Figure S10. Zn plating/stripping from Zn/Zn symmetrical cells at 0.1 mA cm^{-2} in 1 M KOH aqueous electrolyte. In the alkaline electrolyte, there is a gradually increased polarization for Zn plating/stripping performance with a short cycle life within 30 h.

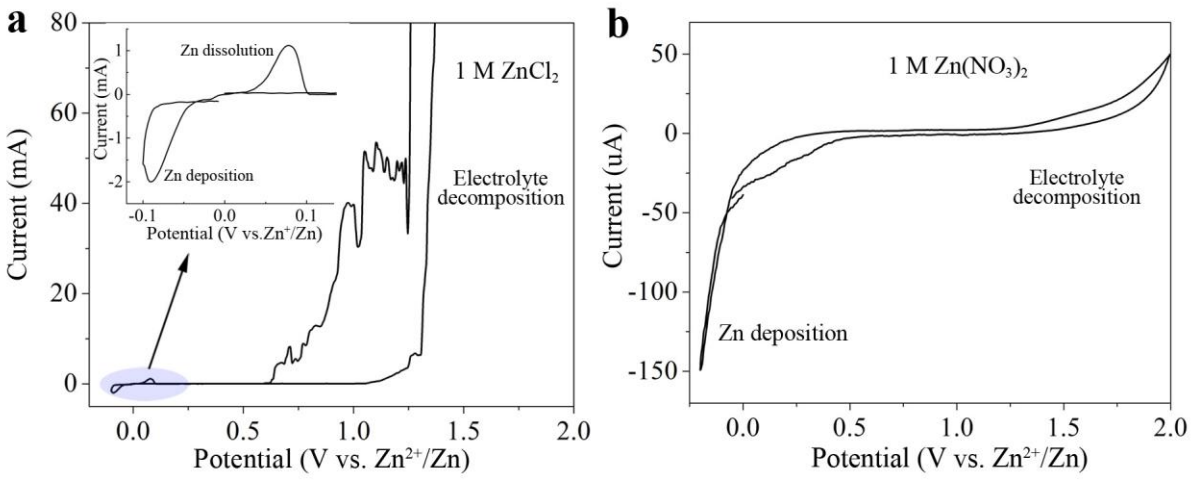

Figure S11. Cyclic voltammograms of Zn electrode in 1 M aqueous electrolyte containing (a) $ZnCl_2$ and (b) $Zn(NO_3)_2$.

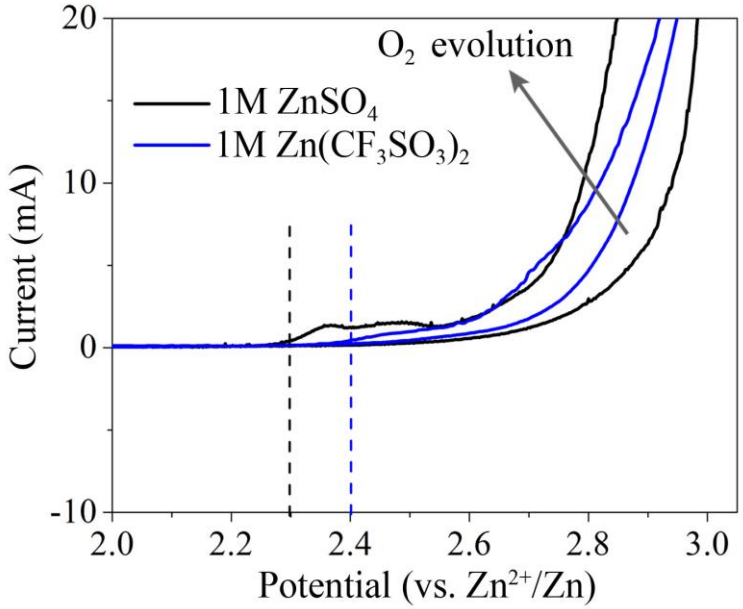

Figure S12. Electrochemical stability for $ZnSO_4$ (1 M, pH = 4.0) and $Zn(CF_3SO_3)_2$ (1 M, pH = 4.9) electrolytes, respectively. The anodic processes for 1 M $ZnSO_4$ and 1 M $Zn(CF_3SO_3)_2$ above 2.3 and 2.4 V can be assigned to the oxygen evolution.

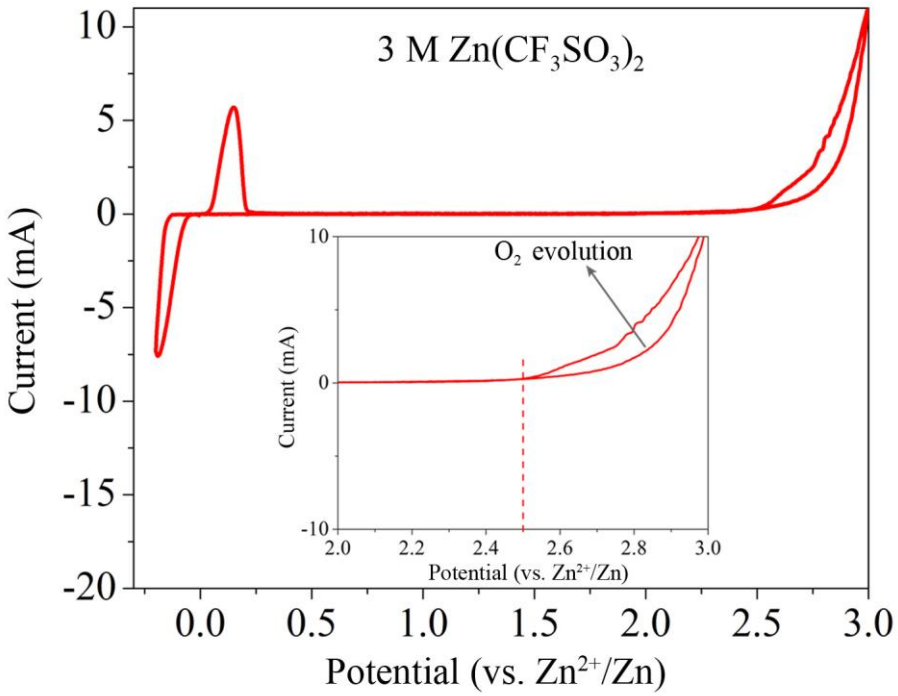

Figure S13. Electrochemical stability for 3 M $Zn(CF_3SO_3)_2$ electrolyte.

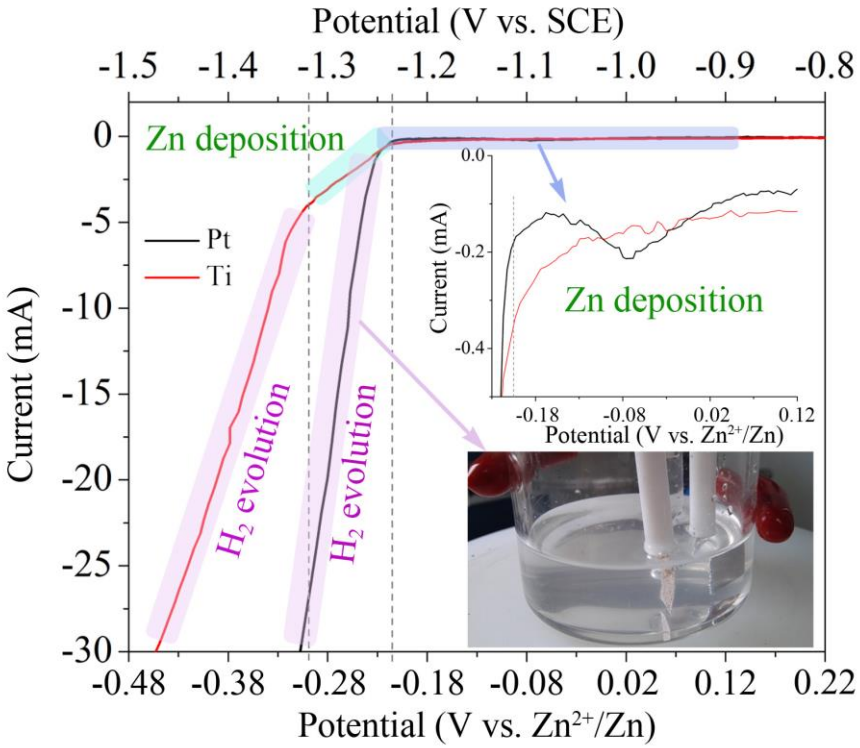

Figure S14. Linear sweeping voltammograms of Pt and Ti foils in 3 M $Zn(CF_3SO_3)_2$ electrolyte using three-electrode cell with platinum plate as the counter electrode and saturated calomel electrode (SCE) as the reference electrode. Inset (upper) shows the enlarged profile of Pt foil. A digital photo shows the three-electrode cell (inset lower) with H_2 gas bubbles on the Pt plate below -0.22 V vs. Zn^{2+}/Zn. For convenience, the potential scale has also been converted to the Zn^{2+}/Zn reference.

The hydrogen evolution reaction (HER) usually occurs on metal (other than Pt) substrates with overpotentials.[7-9] As shown in Figure S14, a larger HER overpotential and lower HER current density at -0.30 V (vs. Zn^{2+}/Zn) were observed on Ti foil as compared to that of Pt plate (-0.22 V vs. Zn^{2+}/Zn). The cathodic process of Ti foil above -0.30 V vs. Zn^{2+}/Zn (light green area) displays much lower slope, which can be attributed to the Zn deposition, consistent with the result of Figure 3a.

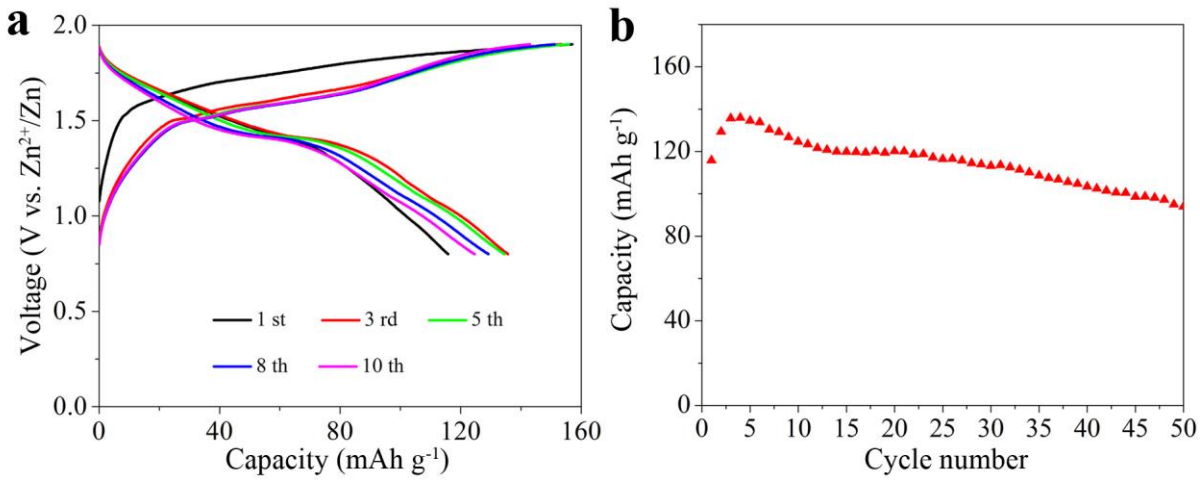

Figure S15. (a) Typical charge/discharge profiles and (b) Cycling performance of ZMO/C at 50 mA g^{-1} in 1 M $Zn(CF_3SO_3)_2$ electrolyte. In such diluted electrolyte, the ZMO/C cathode displays a charge capacity of ~150 mAh g^{-1} after the 3rd cycle, along with a lower Coulombic efficiency than that of ZMO/C in 3 M $Zn(CF_3SO_3)_2$ electrolyte.

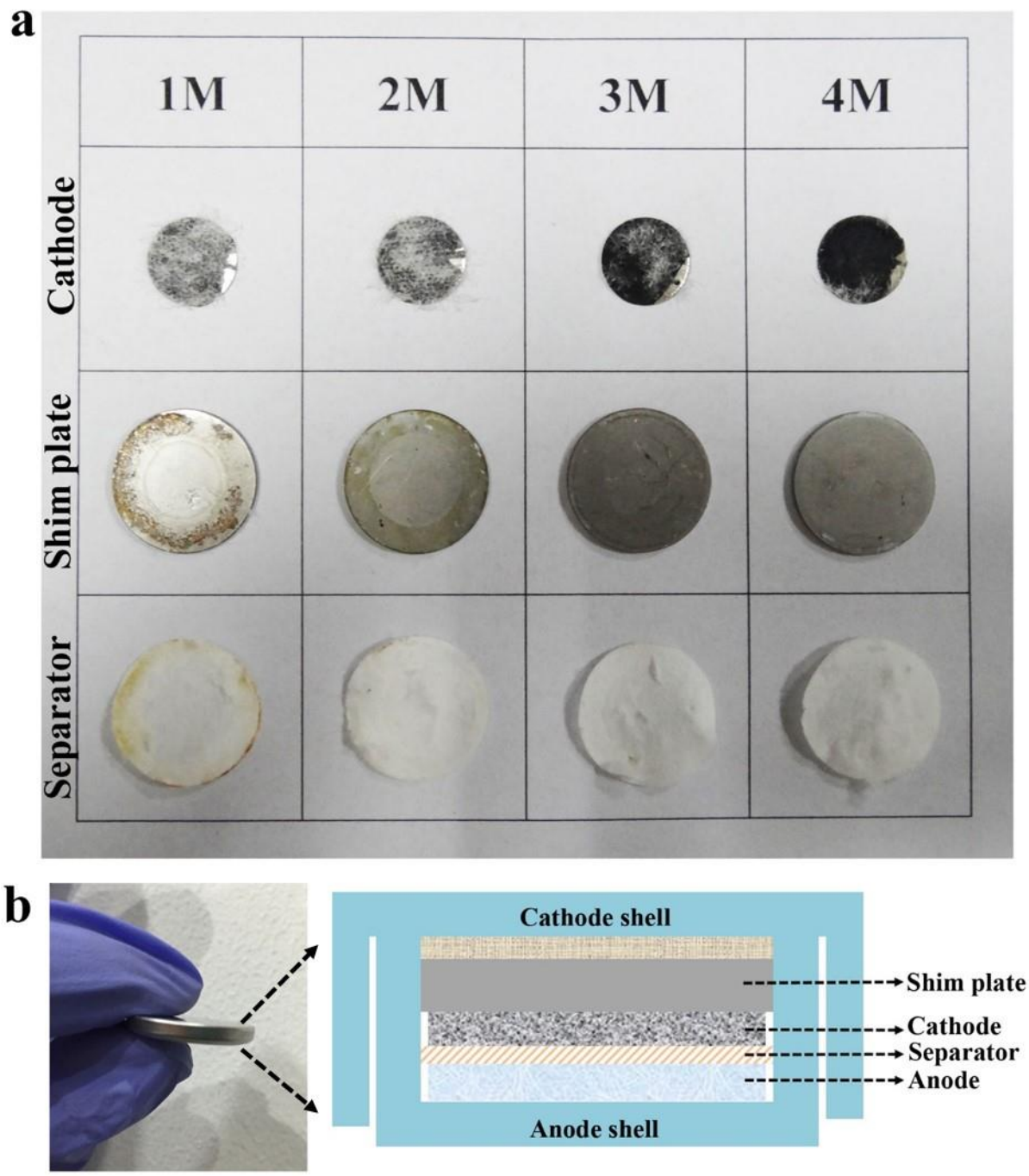

Figure S16. Digital photographs of disassembled cells with electrolytes containing different concentrations (1, 2, 3 and 4 M) of $Zn(CF_3SO_3)_2$. (a) The digital photographs were taken from the cells after 10 charge/discharge cycles. The white fiber adhered on the electrode came from the separator (filter paper), caused by the disassembled process. The peeling of electrode paste was caused by the tweezer. (b) A digital photograph and the corresponding schematic diagram of the coin-type cell.

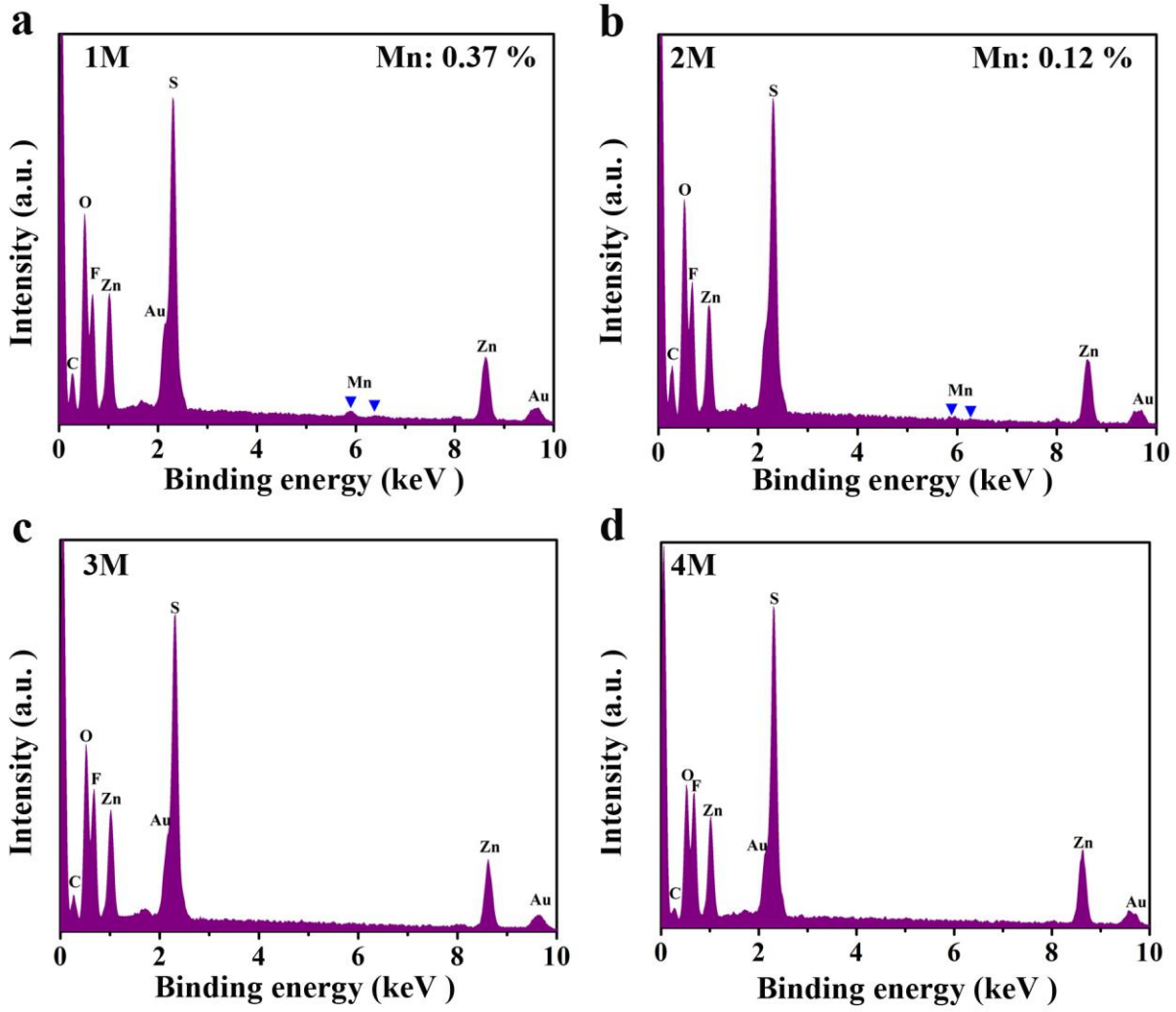

Figure S17. EDS analysis of the separators (filter paper) after 10 charge/discharge cycles with different electrolyte concentrations (1–4 M). EDS analysis was performed through the following process. We disassembled the cells after 10 cycles and obtained the corresponding electrolyte-soaked separators. Then, these separators were dried at 60 ^{o}C for 12 h in vacuum. The separator closed to the anode side was used to conduct EDS analysis.

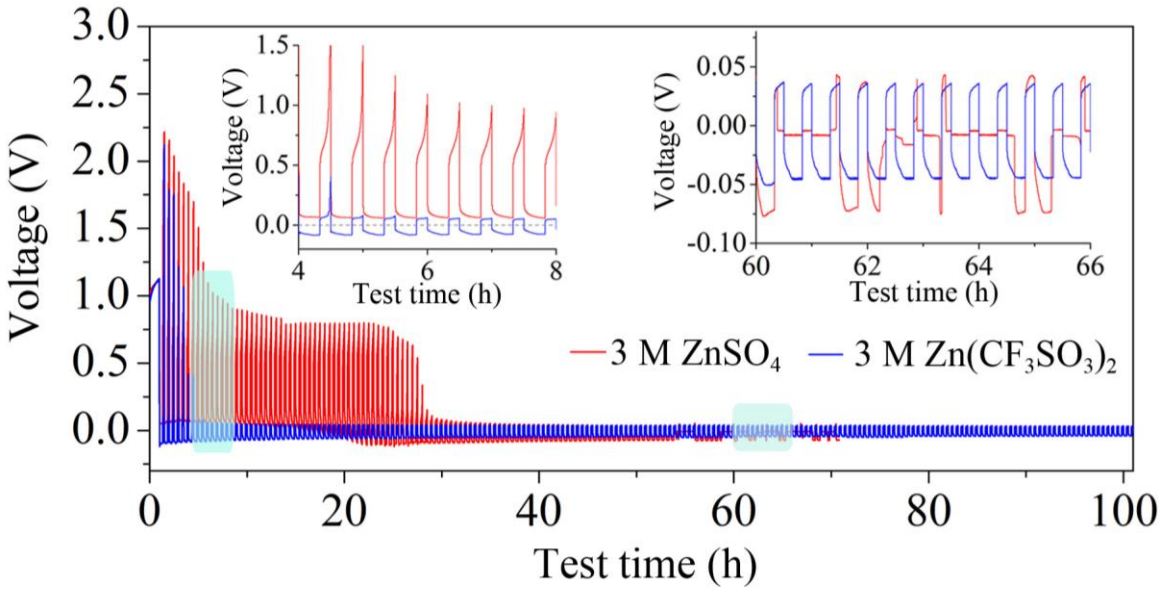

Figure S18. Zn plating/stripping from unsymmetrical Zn/Ti cells at 0.1 mA cm^{-2} in 3 M $ZnSO_4$ and 3 M $Zn(CF_3SO_3)_2$ electrolytes. Insets show the enlarged voltage profiles. In the initial a few cycles, both $Zn(CF_3SO_3)_2$ and $ZnSO_4$ electrolytes show large hysteresis, due to the polarization of the Ti counter electrode. However, after 7 cycles, $Zn(CF_3SO_3)_2$ results in greatly reduced polarization with stable cycling and small hysteresis. In contrast, $ZnSO_4$ undergoes a large polarization until 28 h and only sustains a short duration (< 60 h) of reversible operation.

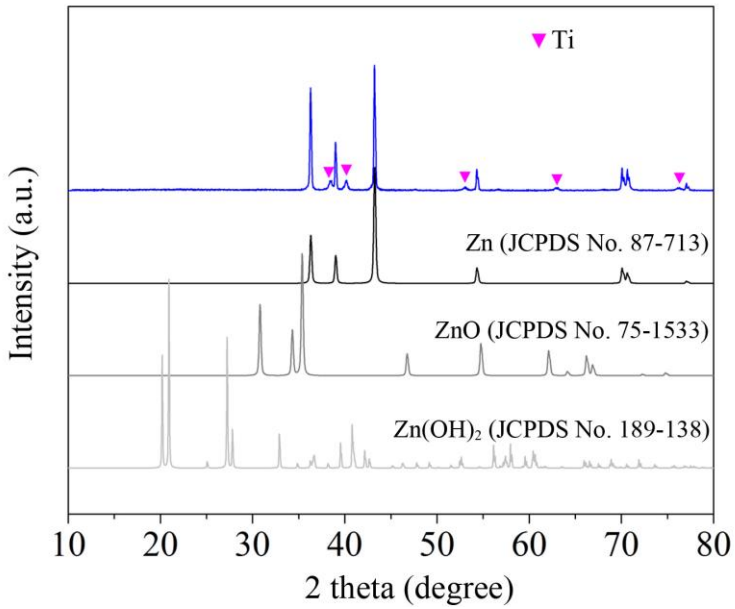

Figure S19. XRD pattern of Zn deposit on Ti foil with metallic Zn, ZnO and $Zn(OH)_2$ as references. The Zn deposit was obtained in 3 M $Zn(CF_3SO_3)_2$ electolyte at -0.2 V vs. Zn^{2+}/Zn, using CV test in a Zn/Ti cell. Clearly, the deposition is metallic zinc without ZnO or $Zn(OH)_2$ byproducts.

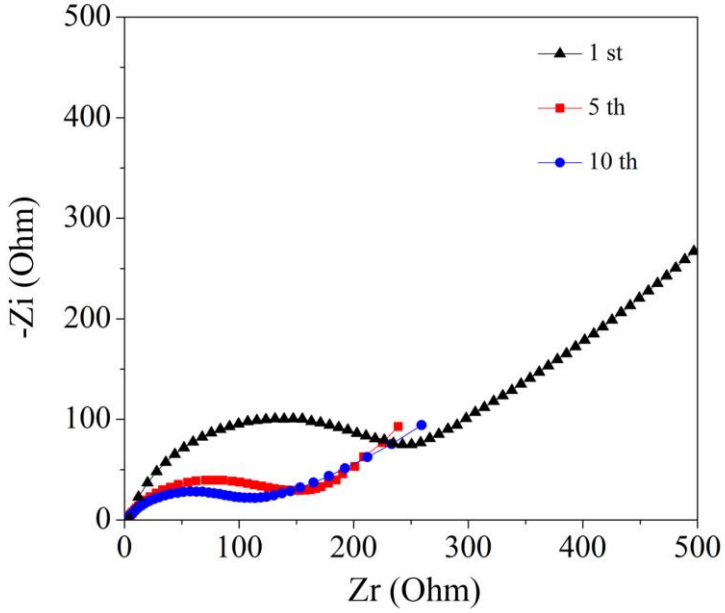

Figure S20. EIS spectra of ZMO/C electrode after 1st, 5th and 10th discharge in 3 M $Zn(CF_3SO_3)_2$. The impedance decreases upon cycling, which contributes to enhanced electrode performance.

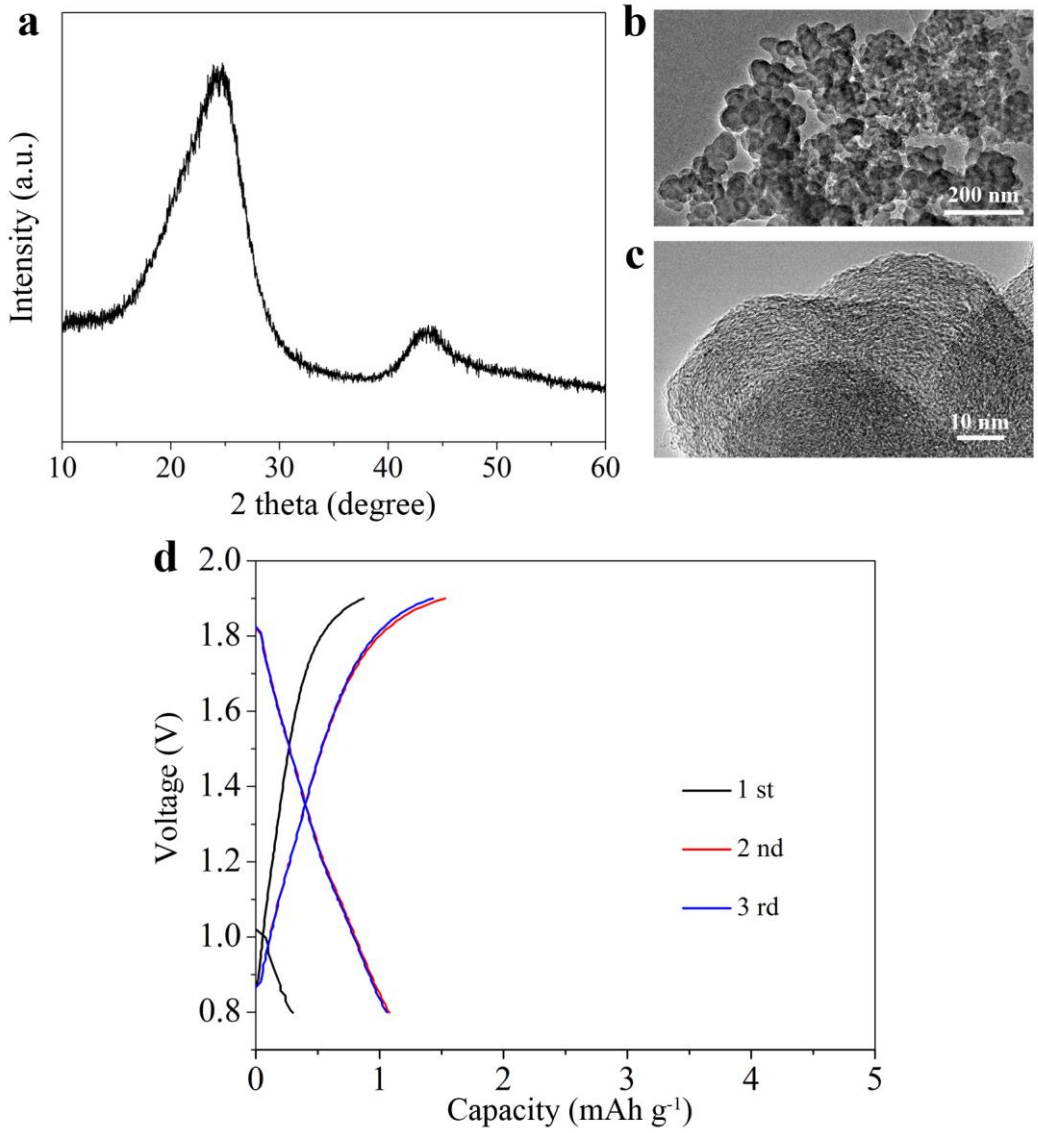

Figure S21. Characterization and electrode properties of carbon (Vulcan XC-72). (a) XRD pattern, (b) TEM image, (c) HRTEM image, and (d) Charge/discharge profiles at 10 mA g^{-1} in 3 M $Zn(CF_3SO_3)_2$. Vulcan XC-72 carbon is widely used as conducting additive or electrocatalyst support.[10,11] This carbon material shows amorphous phase, possesses particle size of 50–100 nm, and delivers negligible capacity even at a low current density of 10 mA g^{-1}.

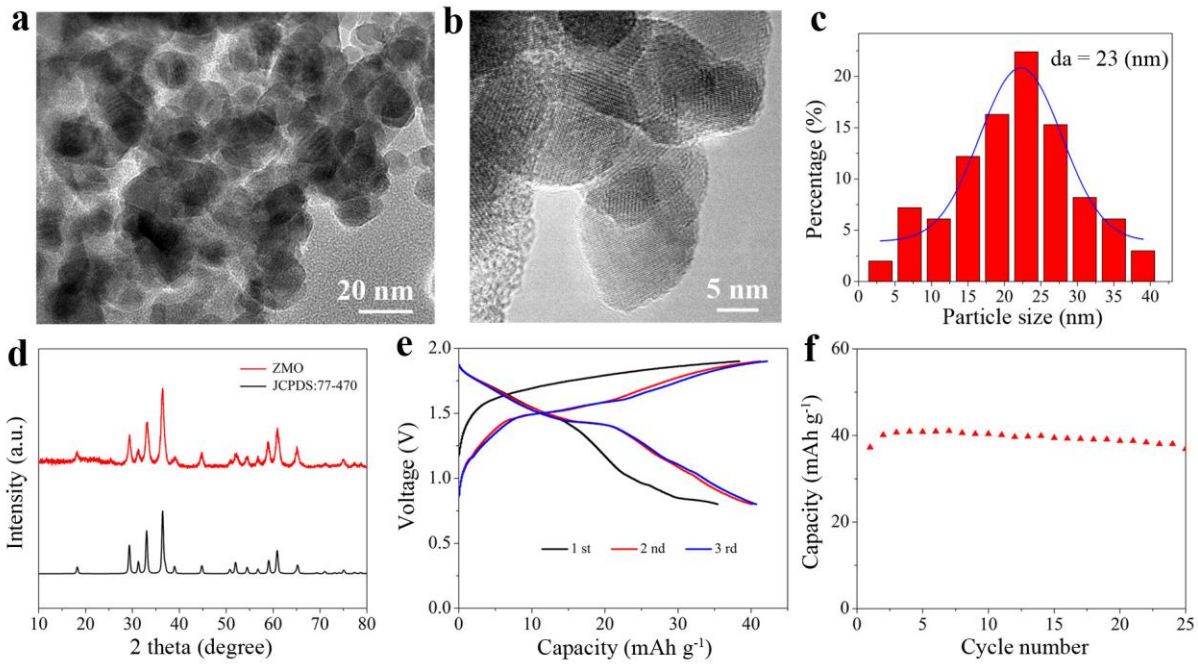

Figure S22. Characterization of nanosized ZMO synthesized from ceramic routes. (a) TEM image, (b) HRTEM image, (c) Particle size distribution histogram, (d) XRD pattern, (e) Charge/discharge curves of ZMO electrode at 50 mA g^{-1} in 3 M $Zn(CF_3SO_3)_2$, and (f) Cycling performance at 50 mA g^{-1}. The ZMO sample has an average particle size of 23 nm. A reversible capacity of ~ 42 mAh g^{-1} is attained after the 3rd cycle. The electrode performance of this 23-nm ZMO is essentially comparable to that of ZMO with average particle size of 50 nm.

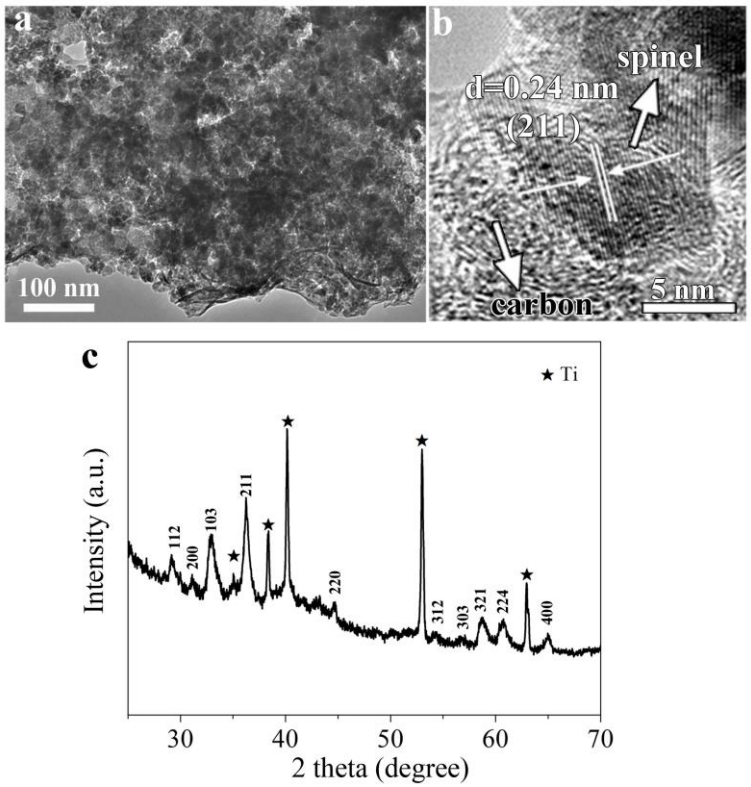

Figure S23. (a) TEM image and (b) HRTEM image of ZMO/C after 50 cycles. The spinel nanoparticles were still firmly anchored on and uniformly composited with carbon. (c) The corresponding XRD pattern of ZMO/C, showing the spinel structure can be well-maintained after cycling.

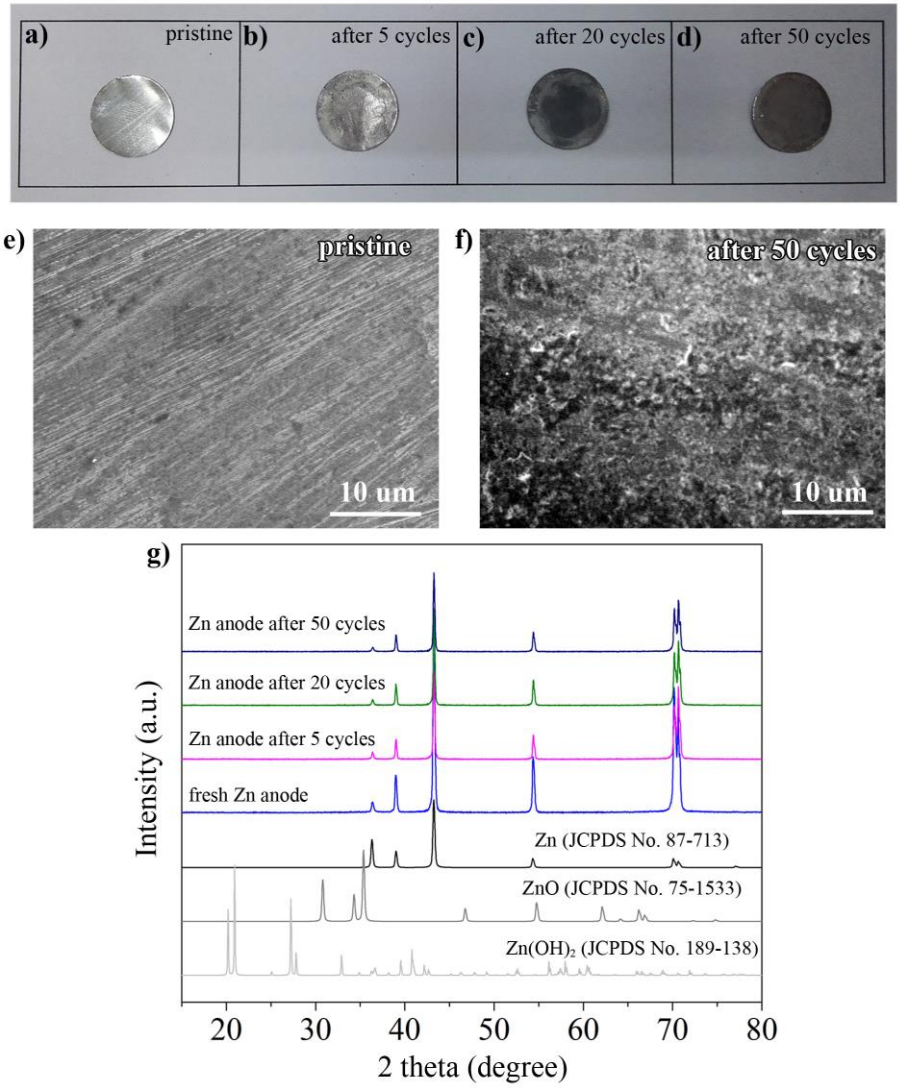

Figure S24. Analysis of Zn anode in Zn-ZMO/C cells. Digital photographs of (a) pristine electrode and cycled electrode after (b) 5 cycles, (c) 20 cycles and (d) 50 cycles. SEM images of (e) pristine electrode and (f) Zn electrode after 50 cycles. (g) XRD patterns of fresh and cycled Zn electrodes with standard patterns of Zn, ZnO and $Zn(OH)_2$ as the reference. The Zn anode shows dendrite-free surface morphology after 50 cycles. Byproduct such as ZnO or $Zn(OH)_2$ is not discernible after cycling.

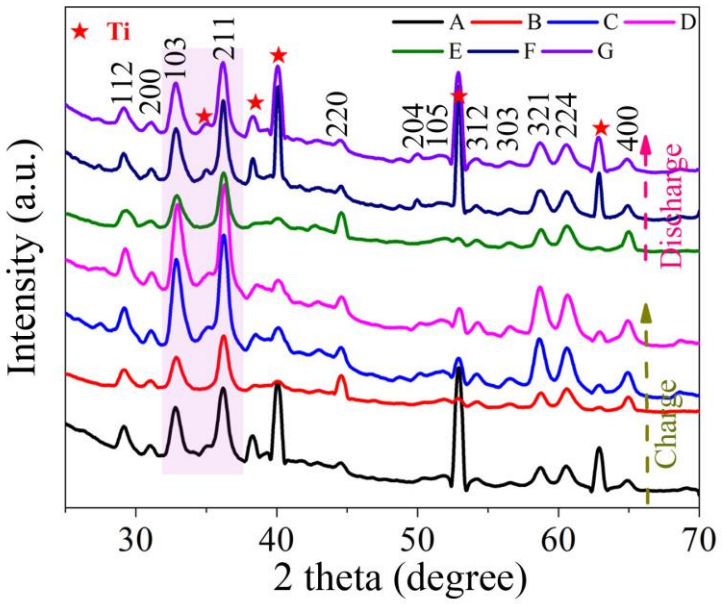

Figure S25. XRD patterns in full 2θ range. XRD patterns of ZMO/C electrodes at selected charge/discharge states as marked in Figure 6a. All discernible peaks can be attributed to the spinel ZMO and the Ti substrate.

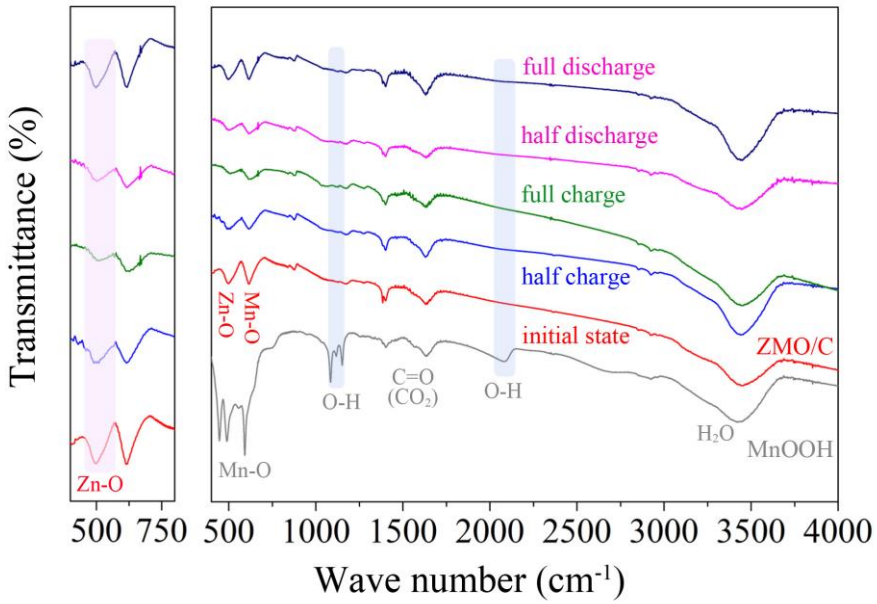

Figure S26. FTIR spectra of ZMO/C electrode at selected charge/discharge states in the 3rd cycle with MnOOH as reference. Before FTIR tests, the electrodes were rinsed with deionized water for 10 times

and dried at 80 ^{o}C for 12 h in vacuum oven.

The preparation of MnOOH followed the similar procedures reported in literature.[12] The broad band at ~3480 cm^{-1} is attributed to the O-H stretching vibrations of the surface-adsorbed water. The three peaks between 1050–1200 cm^{-1} and a broad peak at ~2100 cm^{-1} are typical of the O-H bending modes in the structure of MnOOH.[13] For the initial state of ZMO/C, two strong absorption peaks between 500 and 700 cm^{-1} region correspond to the Zn-O and Mn-O bonding in the spinel structure.[14,15] During charging, the metal-oxygen vibrations, Zn-O bond in particular, are gradually softened, due to the extraction of Zn cations, in line with Raman spectra results. As expected, reverse discharging increases the peak intensity. If proton could insert into the spinel structure, it would interact with oxygen in the spinel. However, O-H bond vibration in the spinel structure could not be observed during the whole process, suggesting that proton insertion can be ruled out.

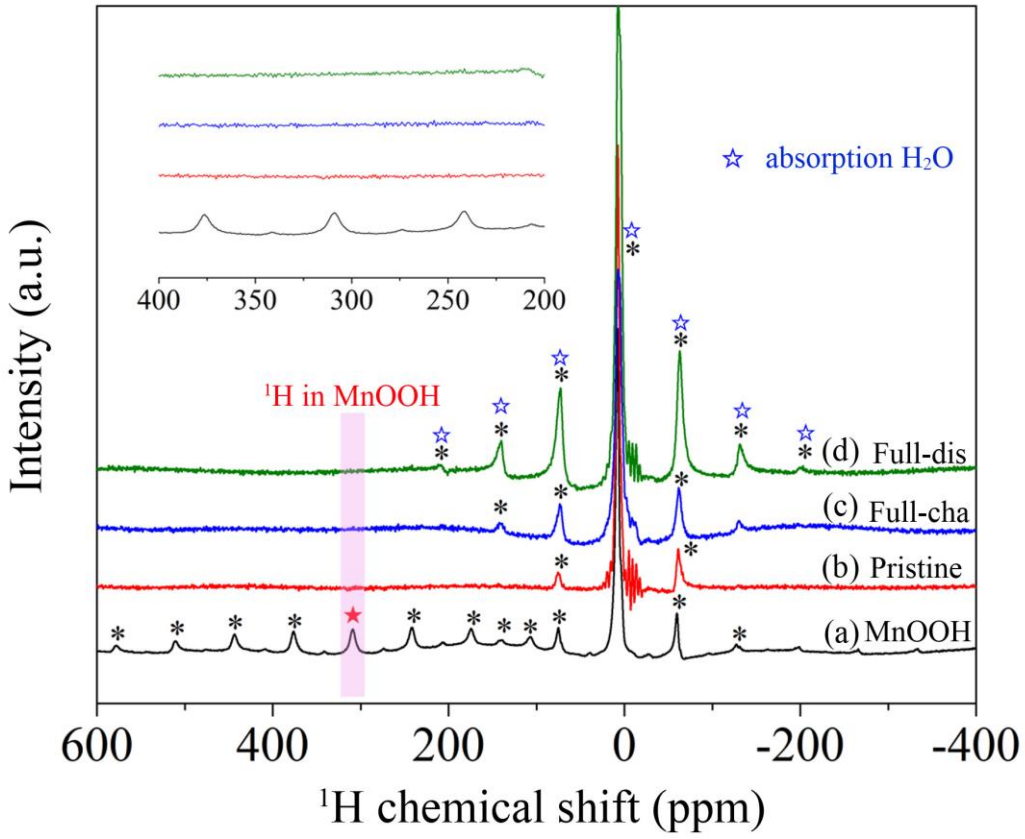

Figure S27. The solid state ^{1}H NMR spectra of (a) MnOOH reference, (b) pristine ZMO/C, (c) full

charged ZMO/C at 3rd cycle, and (d) full discharged ZMO/C at 3rd cycle. Inset shows the enlarged scale profile. A CP/MAS T3 probes with rotor diameter of 2.5 mm was used for 1H fast magic angle spinning (MAS) at 27 kHz. MAS was automatically controlled with a speed controller for all experiments. The ^{1}H chemical shift was referenced to external TMS (0 ppm).

The peaks marked by * are the spinning side bands of isotropic peaks in each NMR spectrum. The ZMO/C cathodes samples were fully charged and fully discharged in the 3rd cycle, respectively. Then, the corresponding cells were disassembled and the recovered cathodes were washed with deionized water. All the samples were dried at 60 ^{o}C for 12 h in vacuum before taking NMR spectra. The isotropic peak located at 310 ppm is assigned to the resonance form MnOOH.[16,17] The isotropic peaks marked as ☆ correspond to absorbed H_2O, due to the NMR test measuring in ambient air. Besides the signals form surface-absorbed water, ^{1}H NMR signals from MnOOH or other ^{1}H peaks could not be observed in both discharged and charged ZMO/C samples, confirming that protons could not intercalate into the spinel structure.

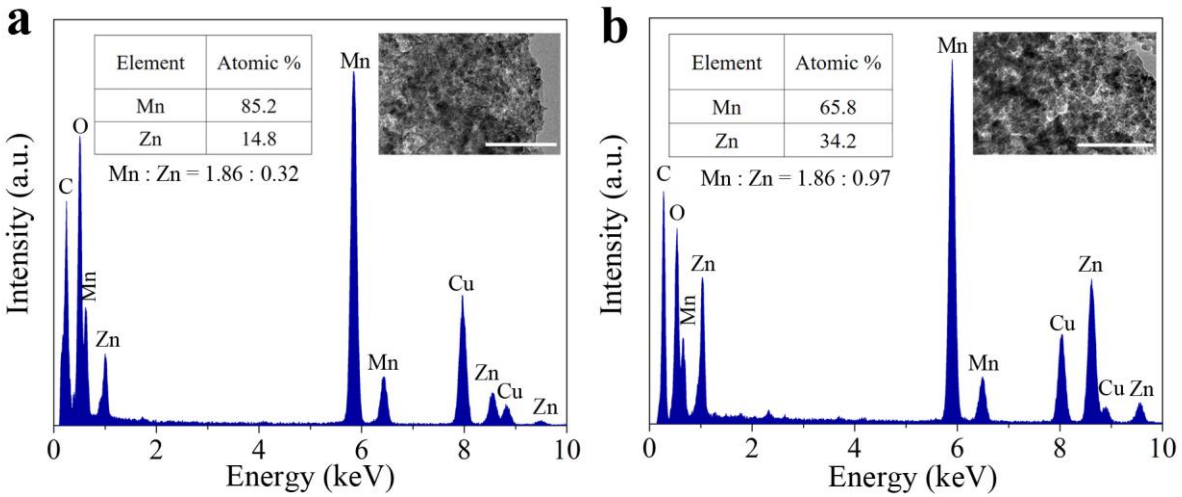

Figure S28. TEM-EDS analysis of ZMO/C at (a) fully charged state and (b) fully discharged state of the 3rd cycle. Insets of (a, b) are the corresponding TEM images and both scale bars are 100 nm. When fully charged, the content of Zn in the cathode apparently decreased and the molar ratio of Mn:Zn was 1.86:0.32. After full discharge, the mass of Zn was recovered and the Mn:Zn molar ratio was increased to 1.86:0.97. This result is consistent with the ICP analysis (Table S5).

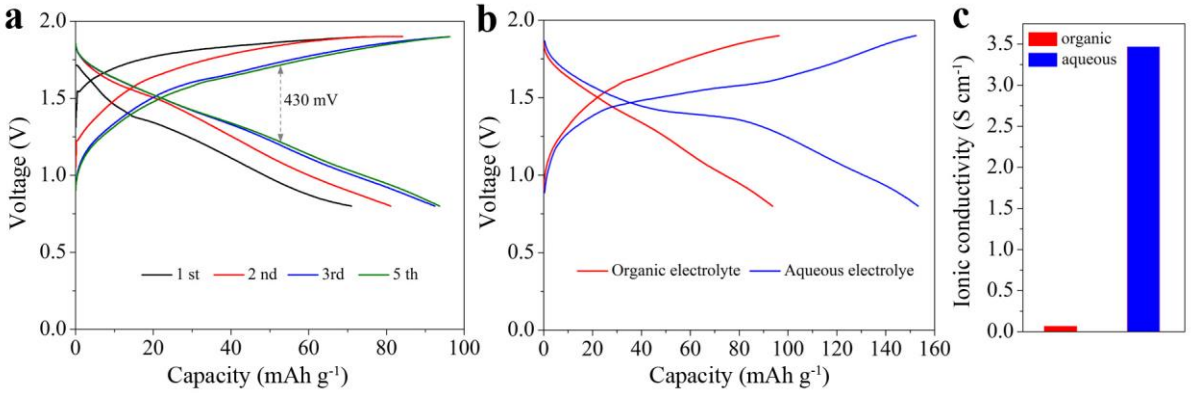

Figure S29. (a) Charge/discharge profiles of ZMO/C electrode in nonaqueous 0.1 M $Zn(CF_3SO_3)_2$/acetonitrile (AN) electrolyte at current density of 20 mA g^{-1}. (b) Comparison of the 5^{th}-cycle charge/discharge profiles of ZMO/C in nonaqueous 0.1 M $Zn(CF_3SO_3)_2$/AN and aqueous 3 M $Zn(CF_3SO_3)_2$ electrolytes. (c) The ionic conductivities of the two electrolytes.

In organic electrolyte without H_2O, the ZMO/C cathode exhibit similar charge/discharge profiles with that in aqueous electrolyte. However, the electrode in nonaqueous electrolyte exhibits lower capacity and large overpotential, possibly due to the significantly lower ionic conductivity of the organic electrolyte as compared to the aqueous electrolyte. The result herein suggests that Zn ions could reversibly extract/insert from/into the spinel structure.

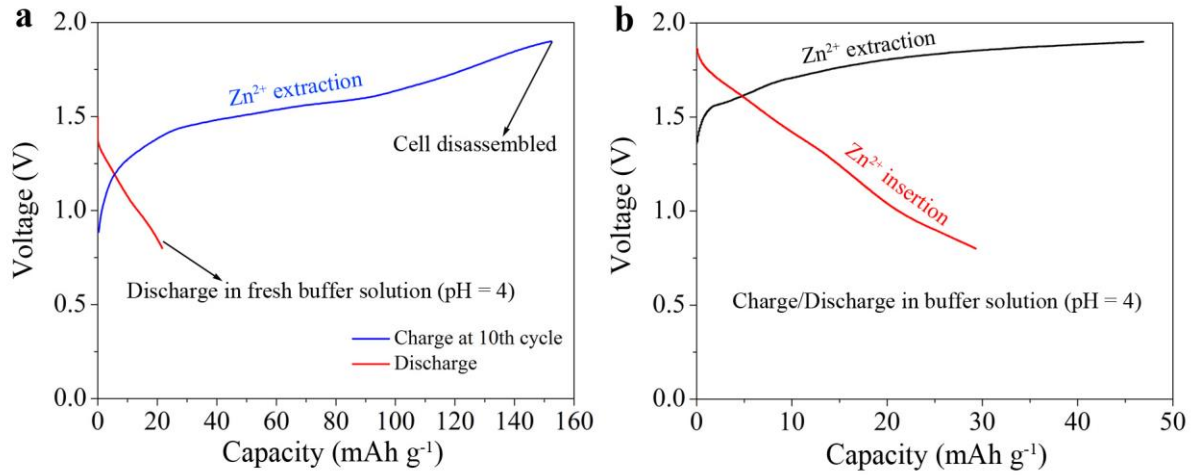

Figure S30. (a) Charge curve (blue) of ZMO/C electrode in the 10th cycle in 3 M $Zn(CF_3SO_3)_2$ electrolyte and discharge curve (red) of dismantled electrode at 20 mA g^{-1} in fresh buffer solution. (b)

Charge/discharge profiles of ZMO/C in buffer solution. The buffer solution was purchased from Lei Ci Company (China), which contains 0.05 M potassium hydrogen phthalate.

A Zn-ZMO/C cell was first cycled at 50 mA g^{-1} for 10 cycles. The cell was disassembled and the electrode at fully charged state was collected. The collected electrode was placed in another cell with fresh buffer solution (pH = 4), with a pH close to that of 3 M $Zn(CF_3SO_3)_2$ electrolyte (pH = 3.6). However, the cell with buffer solution electrolyte could hardly be discharged due to the absence of Zn^{2+} ions. In addition, a fresh Zn-ZMO/C cell using buffer solution (0.05 M potassium hydrogen phthalate) as the electrolye could be charged with a low capacity of 45 mAh g^{-1}, along with even lower amount of insertable Zn ions (Figure S30b). These results indicate that the aqueous acidic buffer solution containing protons other than Zn^{2+} results in very limited capacity as compared to the aqueous 3 M $Zn(CF_3SO_3)_2$ electrolyte, further confirming that proton insertion, even if it exists, contributes negligibly to the capacity of ZMO/C.

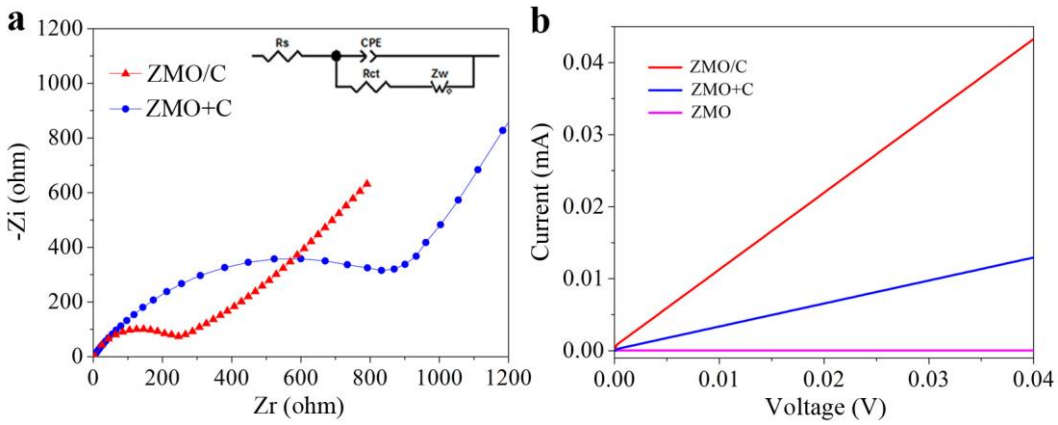

Figure S31. (a) The impedance spectra for ZMO/C and ZMO+C electrodes. Inset: the equivalent circuit (Rs: solution resistance; Rct: charge-transfer resistance; CPE: constant-phase element; Zw: Warburg diffusion process). The charge-transfer resistance of ZMO/C is 280 Ω, which is much lower than that of ZMO+C (1000 Ω). (b) The electrical conductivity measurements for ZMO/C and ZMO+C and neat ZMO. The neat metal oxides ($ZnMn_2O_4$), as insulator, have almost no electrical conductivity. The electrical conductivities are determined to be 2.0 and 0.6 S m^{-1} for ZMO/C and ZMO+C, respectively.

Table S1. XRD refined structural parameters of ZMO/C.

Atom	Site	g	x	y	z
Zn	4a	1	0	0	0
Mn	8d	0.930	0	1/4	5/8
O	16h	1	0	0.2298	0.3745

Space group: I41/amd (No.141). Cell parameter: a=b=5.724 Å, c=9.219 Å. Rwp=3.55%, Rp=2.82%. g: occupancy. x, y and z: atomic coordinates.

Table S2. XRD refined structural parameters of neat ZMO (50 nm).

Atom	Site	g	x	y	z
Zn	4a	1	0	0	0
Mn	8d	1	0	1/4	5/8
O	16h	1	0	0.2476	0.3785

Space group: I41/amd (No.141). Cell parameter: a=b=5.745 Å, c=9.06 Å. Rwp=2.42%, Rp=1.85%. g: occupancy. x, y and z: atomic coordinates.

Table S3. Composition analysis of as-prepared spinels. Mn valence state was determined by chemical titration. (RSD: relative standard deviation)

Samples	Mn valence state	Mn/Zn ratio by EDS analysis	Mn/Zn ratio by ICP analysis	Composition
1	3.22	1.86	1.862	$ZnMn_{1.86}Y_{0.14}O_4$

		(±0.010)	(RSD=0.427%)	
2	3.03	1.98 (±0.015)	1.983 （RSD=0.531%）	$ZnMn_{1.98}Y_{0.02}O_4$

Table S4. Onset potential and Coulombic efficiency (CE) from CV analysis (Figure 2) for $Zn(CF_3SO_3)_2$ and $ZnSO_4$ electrolytes.

1 M $Zn(CF_3SO_3)_2$			
Cycle number	Plating potential (V)	Stripping potential (V)	CE
1st	-0.140	0.050	73%
2nd	-0.110	0.045	96%
3rd	-0.070	0.044	100%
5th	-0.070	0.044	100%
1 M $ZnSO_4$			
Cycle number	Plating potential (V)	Stripping potential (V)	CE
1st	-0.170	0.055	71%
2nd	-0.140	0.052	66%
3rd	-0.130	0.050	53%
5th	-0.110	0.050	48%

Table S5. ICP-AES results of the electrolytes recovered from tested cells after 10 cycles.

Electrolyte	Mn (ppm)	RSD
1 M-Zn$(CF_3SO_3)_2$	10.703	0.3806%
2 M-Zn$(CF_3SO_3)_2$	6.045	0.2696%
3 M-Zn$(CF_3SO_3)_2$	0.1762	0.2480%
4 M-Zn$(CF_3SO_3)_2$	0.1005	0.5637%

The electrolytes were extracted from the tested cells using the following process. The cells were disassembled after 10 cycles. The separators were taken out and immersed in 10 mL deionized water for 30 min at room temperature. The supernatant liquids (5 mL) was collected to perform ICP anaylsis.

Table S6. Summary of electrochemical performance of different cathode materials for ZIBs.

Samples	Electrolyte	Cycling performance	Energy density based on the active electrode materials	Ref.
α-MnO_2 nanorod	1 M $ZnSO_4$	147 mAh g^{-1} at 83 mA g^{-1} with 63% capacity retention after 50 cycles	---	18
α-MnO_2 nanorod	1 M $ZnSO_4$	140 mAh g^{-1} at 42 mA g^{-1} with 70% capacity retention after 30 cycles	~ 157 Wh kg^{-1} after 30 cycles	19
α-MnO_2 nanorod	1 M $ZnSO_4$	100 mAh g^{-1} at 630 mA g^{-1} with 76% capacity retention after 100 cycles	--	20

α-MnO_2 nanorod	2 M $ZnSO_4$ + 0.1 M $MnSO_4$	260 mAh g^{-1} at 308 mA g^{-1} after 60 cycles	---	16
Mesoporous γ-MnO_2	1 M $ZnSO_4$	150 mAh g^{-1} at 0.5 mA cm^{-2} with 60% capacity retention after 40 cycles	---	21
δ-MnO_2 nanoflake	1 M $ZnSO_4$	112 mAh g^{-1} at 83 mA g^{-1} with 45% capacity retention after 100 cycles	---	22
Todorokite-type MnO_2	1 M $ZnSO_4$	98 mAh g^{-1} at 50 mA g^{-1} with 89% capacity retention after 50 cycles	---	23
$Cu_3[Fe(CN)_6]_2$	20 mM $ZnSO_4$	52 mAh g^{-1} at 60 mA g^{-1} with 96% capacity retention after 100 cycles	---	24
$Zn_3[Fe(CN)_6]_2$	1 M $ZnSO_4$	81 mAh g^{-1} at 60 mA g^{-1} with 81% capacity retention after 100 cycles	100 Wh/kg	25
Spinel-$ZnMn_{1.86}O_4$	3 M $Zn(CF_3SO_3)_2$	150 mAh g^{-1} at 50 mA g^{-1} with ~100% capacity retention after 50 cycles 80 mAh g^{-1} at 500 mA g^{-1} with 94% capacity retention after 500 cycles	202 Wh/kg after 50 cycles	This work

Table S7. The fit data for ex situ Raman analysis.

States	Peak position (cm^{-1})	FWHM (cm^{-1})

A	665.64	22.55
B	666.83	44.74
C	668.03	63.62
D	672.64	78.74
E	669.20	64.68
F	667.18	45.76
G	666.14	30.65

Table S8. Mn/Zn ratio analysis of ZMO/C at different states.

State	Mn/Zn ratio by ICP analysis
Full charge	1.86 : 0.34 (Mn 488.6 ppm; Zn 89.3 ppm)
Full discharge	1.86 : 0.38 (Mn 472.4 ppm; Zn 248.9 ppm)

References

1. Zeng, Z.; Greenblatt, M.; Croft, M. *Phys. Rev. B* **1999**, *59*, 8784.
2. Sanchez, L.; Pereira-Ramos, J. P. *J. Mater. Chem.* **1997**, *7*, 471.
3. Cheng, F.; Shen, J.; Peng, B.; Pan, Y.; Tao, Z.; Chen, J. *Nat. Chem.* **2011**, *3*, 79.
4. Du, J.; Zhang T.; Cheng, F.; Chu, W.; Wu, Z.; Chen, J. *Inorg. Chem.* **2014**, *53*, 9106.
5. Xie, J.; Kohno, K.; Matsumura, T.; Imanishi, N.; Hirano, A.; Takeda, Y.; Yamamoto, O. *Electrochim. Acta.* **2008**, *54*, 376.
6. Shaju, K.; Subba, G.; Chowdari, B. *J. Mater. Chem.* **2003**, *13*, 106.
7. Liang, Y. Y.; Li, Y. G.; Wang, H. L.; Dai, H. J. *J. Am. Chem. Soc.* **2013**, *135*, 2013.
8. Lukowski, M.; Daniel, A.; Meng, F.; Forticaux, A.; Li, L.; Jin, S. *J. Am. Chem. Soc.* **2013**, *135*, 10274.

9. Zhao, Y.; Wang, E.; Jiang, L.; Sun, G. *RSC Adv.* **2015**, *5*, 83781.
10. Li, C.; Han, X.; Cheng, F.; Hu, Y.; Chen, C.; Chen, J. *Nat. Commun.* **2015**, *6*, 7345.
11. Gorlin Y.; Jaramillo T. *J. Am. Chem. Soc.* **2010**, *132*, 13612.
12. Y. Zhang, Y. Liu, F. Guo, Y. Hu, X. Liu, Y. Qian, *Solid State Commun.* **2005**, *134*, 523.
13. Bayoudh, A.; Etteyeb, N.; Kossai, R. *Ceram. Int.* **2015**, *41*, 12273.
14. Lobo, L.; Kumar, A. *J. Mater. Sci: Mater. Electron.***2016**, *27*, 7398.
15. Deng, Y.; Tang, S.; Zhang, Q.; Shi, Z.; Zhang, L.; Zhan, S.; Chen, G. *J. Mater. Chem*. **2011**, *21*, 11987.
16. Pan, H.; Shao, Y.; Yan, P.; Cheng, Y.; Han, K. S.; Nie, Z.; Wang, C.; Yang, J.; Li, X.; Bhattacharya, P.; Mueller, K. T.; Liu, J. *Nat. Energy* 2016, *1*, 16039.
17. Paik, Y.; Osegovic, J.; Wang, F.; Bowden, W.; Grey, C. *J. Am. Chem. Soc.* **2001**, *123*, 9367.
18. Alfaruqi, M.; Gim, J.; Kim, S.; Song, J.; Jo, J.; Kim, S.; Mathew, V.; Kim, J. *J. Power Sources* **2015**, *288*, 320.
19. Lee, B.; Lee, H. R.; Kim, H.; Chung, K. Y.; Cho, B. W.; Oh, S. H. *Chem. Commun.* **2015**, *51*, 9265.
20. Xu, C.; Li, B.; Du, H.; Kang, F. *Angew. Chem. Int. Ed.* **2012**, *51*, 933.
21. Alfaruqi, M. H.; Mathew, V.; Gim, J.; Kim, S.; Song, J.; Baboo, J. P.; Choi, S. H.; Kim, J. *Chem. Mater.* **2015**, *27*, 3609.
22. Alfaruqi, M.; Gim, J.; Kim, S.; Song, J.; Pham, D.; Jo, J.; Xiu, Z.; Mathew, V.; Kim, J. *Electrochem. Commun.* **2015**, *60*, 121.
23. Lee, J.; Ju, J.;Cho, W.; Cho, B.; Oh, S. *Electrochim. Acta.* **2013**, *112*, 138.
24. Trócoli, R.; La Mantia, F. *ChemSusChem* **2015**, *8*, 481.
25. Zhang, L.; Chen, L.; Zhou, X.; Liu, Z. *Adv. Energy Mater*. **2015**, 5, 1400930.